INNSPUB

Journal of Biodiversity and Environmental Sciences (JBES)
ISSN: 2220-6663 (Print) 2222-3045 (Online)
Vol. 25, No. 1, p. 10-25, 2024
http://www.innspub.net

RESEARCH PAPER OPEN ACCESS

Development of Cu-Fe loaded activated porous carbon ($CuFe_2O_4$/AC nanocomposite) using sugarcane bagasse for photodegradation, antimicrobial activity and dye adsorption by batch kinetic studies

T. Madhumitha[1], M. Margret Leema[2], E. Amutha[1], E. Pushpalakshmi[1], M. Earnest Stephen Gnanadoss[4], S. Rajaduraipandian[3], G. Annadurai[*1]

[1]*Sri Paramakalyani Centre of Excellence in Environmental Sciences, Manonmaniam Sundaranar University, Alwarkurichi, India*

[2]*Department of Chemistry, Arignar Anna College, Manonmaniam Sundaranar University, Aralvoimozhi, India*

[3]*Sri Paramakalyani College, Manonmaniam Sundaranar University, Alwarkurichi, India*

[4]*Department of Physics, Sri Venkateswara College of Engineering and Technology, Chittoor, Andra Pradesh, India*

Article published on July 05, 2024

Key words: $CuFe_2O_4$, Activated carbon, Hydrothermal, Photocatalysis and energy storage, Adsorption, Methylene blue dye, Kinetic studies

Abstract

A novel hydrothermal method has been utilized to synthesize Cu Fe_2O_4/AC Nanocomposite that avoids any usage of surfactants. Wherein, Cu Fe_2O_4/AC Nanoparticle was synthesized in the temperature range between 120 to 180°C by hydrothermal method and results a greater reproducibility. The synthesized Cu Fe_2O_4/AC Nanocomposite and Characterized by SEM, XRD, FTIR, TGA, Cyclic Voltammetry (CV), Electrostatic Impedance Spectroscopy (EIS), Electrostatic impedance spectroscopy (EIS) studies. Studies on the antibacterial activity and photocatalytic degradation of a chemically generated Cu Fe_2O_4/AC nanocomposite were also carried out. The Kinetic model better fits the experimental findings of the Cu Fe_2O_4/AC Nanocomposite. The kinetic adsorption results were studied using pseudo-first- and pseudo-second-order models. The second-order models primarily regulated the adsorption rate and exhibited a high correlation coefficient ($R^2 > 0.99$). Cu Fe_2O_4/AC Nanocomposite usually absorbs anions during the adsorption process of Methylene blue because, at acidic pH values, an increase in positively charged regions creates attractive electrostatic forces. The results of this investigation demonstrate that the Cu Fe_2O_4/AC Nanocomposite effectively extracts the Methylene blue dye from the aqueous solution; hence, the Cu Fe_2O_4/AC Nanocomposite exhibits a low rate of degradation during repeated use.

***Corresponding Author:** G. Annadurai ✉ gannadurai@msuniv.ac.in

Introduction

In the past few decades, activated carbons have found widespread use in energy storage and pollution control applications, including purification and separation processes (Choi, 2010; Huang *et al.,* 2014, Sarasidis *et al.,* 2017), toxic substance removal (Gokce and Aktas, 2014), gas storage (Sawant *et al.,* 2017), and supercapacitors wastewater treatment (Jin *et al.,* 2023; Xia *et al.,* 2023). High surface area and porosity, superior adsorption capacity, effective electrical qualities, eco-friendliness, cheap cost, and absence of secondary contamination are all necessary for these applications. The production of activated carbon to fulfill the demands of commercial applications has various advantages, as demonstrated by recent technological breakthroughs. The raw ingredients and the activation technique affect the properties of activated carbon (Boudrahem *et al.,* 2011). Improvements in surface chemistry with respect to functional groups and adsorption capacity, as well as pore structure and volume, surface areas, and improvements have been brought about by technological advancements (Lozano-Castello *et al.,* 2001). Researchers are working harder to find ways to produce Activated carbon from waste materials generated by agriculture and industry. Utilizing waste byproducts has benefits due to their accessibility and affordability. Numerous agricultural by-products with a high carbon and low ash content can be converted into Activated carbons. These include pineapple crown waste (Taer *et al.,* 2019), coconut shells (Mi *et al.,* 2012), rice husk (Mohanty *et al.,* 2006), coffee residue (Khenniche *et al.,* 2010), bamboo (Liu *et al.,* 2010), palm shell (Onundi *et al.,* 2010), and olive stones (Budinova *et al.,* 2006). In general, there are two established processes for making activated carbon: chemical activation and physical activation. Chemical activation combines the processes of carbonization and activation in one step. First, the raw material is impregnated with dehydrating chemicals like H_3PO_4, $ZnCl_2$, K_2CO_3, NaOH, or KOH. Next, it is carbonized at the appropriate temperature in an inert atmosphere (Mohammadi *et al.,* 2010). The process involves carbonizing the raw material and then placing it in an oxidizing gas atmosphere of CO_2 (Sekirifa *et al.,* 2013), water steam (Zhou *et al.,* 2018), air, or some combination of these activating agents under a moderately high temperature (800–1100 °C) to improve the internal structure. As a result, carefully crafted activated carbon materials have demonstrated the ability to adsorb a wide spectrum of heavy metals and different kinds of electrode material. Lead, copper, zinc, chromium, cadmium, and mercury are examples of heavy metals that can have a negative impact on the environment and human health. At the moment, activated carbon is the most widely used adsorbent, and adsorption is thought to be one of the simplest and most efficient methods. Developing extremely specialized carbon types that are ideal for particular industry applications is one of the main challenges in the production of activated carbon. Activated carbon finds additional environmental use in energy storage applications, including the electrodes of supercapacitor devices, where it can be customized to fit different electrolytes with its large, pore-shaped surface area. The objective of this study is to create affordable activated carbon by employing sugarcane bagasse, a form of agricultural waste, and physical activation with CO_2 to prevent additional contaminants from chemicals used in the activation process. Scanning electron microscopy (SEM), X-ray Diffraction, Cyclic Voltammetry (CV), Electrostatic Impedance Spectroscopy (EIS), Thermogravimetric analysis (TGA), and Fluorescence Thermoelectric Reflectance (FTIR) were used to evaluate the Cu Fe_2O_4/AC nanoparticles. The main uses include photodegradation, antibacterial applications, and adsorption studies. Through the fitting and computation of kinetic models from adsorption investigations, the adsorption capacity of dye from an aqueous solution was examined, taking into account the effects of doses, pH, and temperature.

Materials and methods

All of the compounds were used without further purification because they were all AR grade. Sigma-Aldrich, an Indian company, supplied the following chemicals: copper chloride, ferric chloride, sodium hydroxide, Methyelene blue, carbon black, nickel

foam, N-methyl-2-pyrrolidone, potassium hydroxide, and carbon black.

Fig. 1. Preparation of activated carbon

Synthesis of activated porous carbon from sugarcane bagasse

From a sugarcane selling location in Kadayam, sugarcane bagasse was gathered. The raw sugarcane bagasse was chopped into small pieces, cleaned multiple times in DI water, and then dried for 48 hours in the sun before spending 24 hours in a hot air oven at 80°C. Next, as indicated in Fig. 1, the dried sugarcane bagasse was finely ground with a mortar and pestle before being carbonized for four hours at 400° C in a muffle furnace.

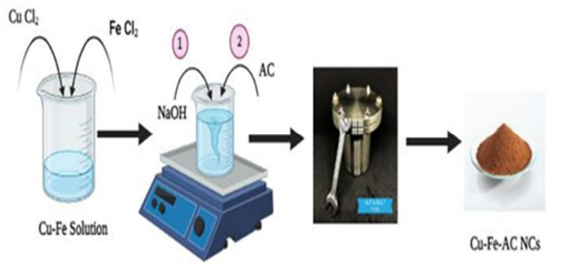

Fig. 2. Synthesis of Cu Fe_2O_4/AC nanocomposite

Synthesis of copper ferrite/activated carbon nanocomposite (Cu Fe_2O_4/AC nanocomposite)

Using a hydrothermal process, the copper ferrite (Cu Fe_2O_4)/activated carbon composite was created. First, 30 mL of deionized (DI) water was used to dissolve 0.023 g of copper chloride and 0.054 g of ferric chloride (1:2 molar ratio), which were then agitated for 30 minutes. After that, this mixture received 0.04 g of NaOH and was agitated for one hour. A 1-hour sonication was performed on 10 mL of DI water containing 0.05 g of Activated carbon. After that, for a full hour, both solutions were combined and swirled. After that, 25 mL of the mixture was placed in a 50 mL Teflon-lined stainless-steel autoclave and heated to 180°C for fifteen hours. After centrifuging the produced precipitate, ethanol and DI water were used several times to clean it. The precipitate as prepared was centrifuged and then repeatedly cleaned with DI water and ethanol. After washing, the sample was dried for a whole night at 100°C in an oven. As seen in Fig. 2, the dried sample was calcined at 60°C for three hours.

Photocatalytic activity

By observing the photocatalytic degradation of Methylene blue dye under UV irradiation, the photocatalytic performance of the Cu Fe_2O_4/AC Nanocomposite was assessed. Typically, 100 mL of an aqueous solution of Methylene Blue dye with an initial concentration of 1 ppm was mixed with 0.1 g of Cu Fe_2O_4/AC Nanocomposite. To attain adsorption/desorption equilibrium, the suspension containing the dye solution and Cu Fe_2O_4/AC Nanocomposite was agitated in the dark for thirty minutes prior to irradiation. Next, UV light was applied to the suspension. About 2 mL of the suspension was removed from the combination every 30 minutes during the irradiation process, and the photocatalyst particles were separated by centrifuging the suspension. A UV-vis spectrophotometer was then used to quantify the concentration of Methylene blue dye solution, which has a distinctive absorption at λmax - 668 nm, in the supernatant. A spectrophotometer was used to measure the transparent liquid at 668 nm after the solutions were centrifuged. The degradation efficiency was calculated using the mentioned-below formula:

$$\text{Degradation efficiency } (\%) = (C_I\text{-}C_F/C_I) \times 100 \quad (1)$$

Where, C_I and C_F are the liquid-phase concentrations of dye at initial and final concentration (g/L)

Agar well diffusion assay

Using pathogenic bacteria such as Gram-positive *Staphylococcus aureus (a) and Bacillus subtilus (b),* as well as Gram-negative *Escherichia coli (c), Enterobacter (d), and Pseudomonas fluorescens (e),* the antibacterial property of the Cu Fe_2O_4/AC

Nanocomposite was ascertained through the application of the well diffusion method. Various concentrations were employed to determine the antimicrobial activity of the aforementioned bacterial species: 25µl, 50µl, 75µl, and 100µl. Following a 24-hour incubation period at 37°C, the zone of inhibition of bacteria on each plate was assessed.

Sorption studies and kinetics

The following batch approach was used to determine the experimental data (Crini *et al.,* 2006; 2007; Gregorio, 2008) In each experiment, 100 mL of an aqueous dye solution at a known concentration at various dosages (0.1, 0.2, and 0.3 g/L), pH (5.5, 6.8, 7.8), and temperatures (30°C, 45°C and 60°C) was combined with 0.1g/L of Cu Fe_2O_4/AC Nanocomposite. The flask was firmly covered. The adsorption of dyes on polymers is greatly enhanced by the presence of inorganic salt (Crini *et al.,* 2006; 2007; Gregorio, 2008). Either HCl or NaOH was used to bring the pH down to 8. At 30°C, the solution was agitated using a revolving shaker. A UV- Visible Spectrophotometer was then used to detect the dye concentration in solution at different time intervals by using spectrophotometry. Every experiment was carried out in triplicate with the same setup and was determined to be repeatable. To find out how the initial dye concentration in the solution affected the adsorption capacity, the dye concentration was changed. Additionally, investigations were carried out over a range of time intervals to ascertain the point at which the maximum amount of dye was adsorbed and the adsorption equilibrium was established. The mass balance equation provided by allowed for the calculation of the amount of dye adsorbed at equilibrium (q_e):

$$q_e = \frac{C_I - C_F}{m} \times v \qquad (2)$$

Where C_I is the initial dye concentration in liquid phase (g/L); C_F is the liquid phase dye concentration at equilibrium (g/L); V is the volume of dye solution used (L); and m is the mass of sorbent used (g).

Results and discussion

Ultraviolet (UV) spectroscopy

To investigate the optical properties of Cu Fe_2O_4/AC Nanocomposite, the UV–vis spectra were measured (Fig. 3). Cu Fe_2O_4/AC Nanocomposite have a characteristic surface plasmon resonance (SPR) band of Cu-Fe between 200 and 1100 nm, with a peak about 340 nm in the absorption spectra (Gregorio, 2008).

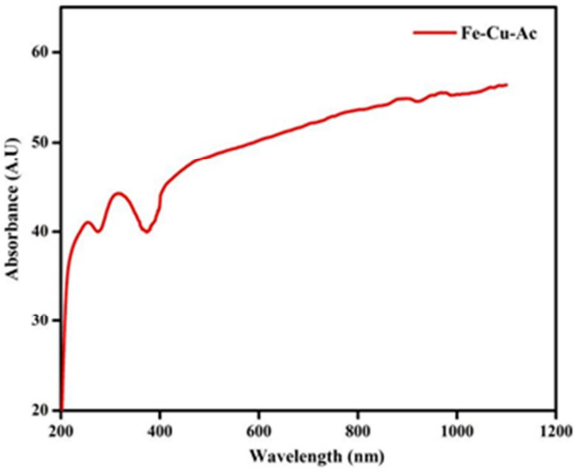

Fig. 3. Optical spectrum of Cu Fe_2O_4/AC nanocomposite

The carbon-coated iron and copper nanoparticles disperse efficiently in liquids and remain generally stable for up to three months, as seen by the solution's black colour.

X-ray diffraction (XRD)

Fig. 4 displays the X-ray diffraction pattern of the Cu Fe_2O_4/AC Nanocomposite, which was produced via a chemical process. Diffraction peaks were discovered at 34°, 38°, and 64°, which corresponded to the crystallographic planes (111), (200), and (220), respectively. The Cu Fe_2O_4/AC Nanocomposite, which has a face-centered cubic structure, is represented by these diffraction peaks (JCPDS Card No. 04-0783) (Amit *et al.*, 2016). There are a few extra peaks since the material has crystalline flaws. These studies demonstrated the conversion of Cu-Fe ions to Cu-Fe nanoparticles by the NaOH. X-ray diffraction was used to quantify and confirm the nanoparticles' crystal size using Scherer's formula.

The estimated particle size was about 24 nm, in agreement with findings from scanning electron microscopy (Hang *et al.*, 2011).

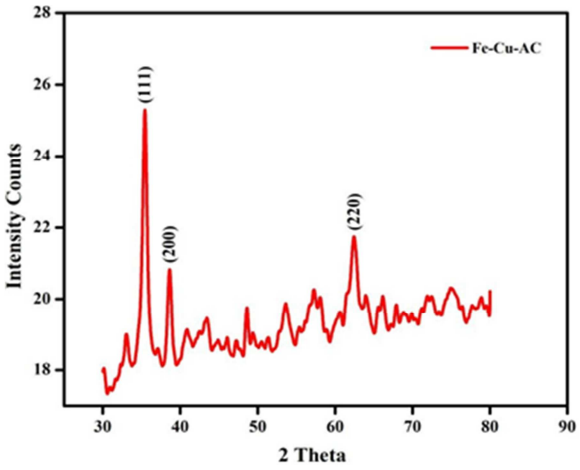

Fig. 4. XRD spectrum of Cu Fe_2O_4/AC nanocomposite

Dynamic light scattering (DLS)

Cu Fe_2O_4/AC Nanocomposite was treated with ultrasonography and then suspended in ethanol. Using a particle size analyzer (PSA), the diameters of the agglomerated colloids in the suspensions were calculated. The measured particle size of 54 nm is in good agreement with the twice-larger crystallite size of Cu-Fe NPs (Ahn *et al.,* 2004). Fig. 5 displays the average and distribution of particle sizes for the Cu Fe_2O_4/AC Nanocomposite. A coherent light source is aimed at a suspension of particles in DLS, and the light is scattered there.

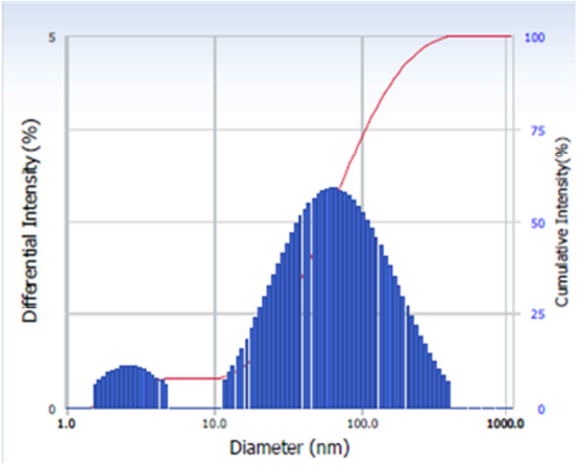

Fig. 5. DLS image of Cu Fe_2O_4/AC Nanocomposite

The scattering varies over time as a result of the particles' random Brownian motion and the ever-changing distances between the scatterers. When Cu Fe_2O_4/AC Nanocomposite is analyzed, the size of ionic liquid and activated carbon mediated nanocomposites as determined by DLS may look smaller than chemical mediated nanoparticles without ionic liquid. Activated carbon-mediated nanocomposites clump together quickly in the majority of investigations. In this study, DLS is seen four hours after aging. Previously, the size distribution profile of nanoparticles in suspension was established using DLS.

Fourier transforms infrared (FTIR) spectroscopy

Fig. 6 displays the results of an FTIR analysis used to describe the Cu Fe_2O_4/AC nanocomposite that was extracted from the plant. The wave number range for FTIR analysis is 450/cm to 4000/cm. Prominent bands of absorbance were seen at approximately 3432, 2923, 2853, 1633, 1445, 1024, and 584 cm−1 in all three Cu Fe_2O_4/AC nanocomposite solutions (Piyush *et al.,* 2018). As indicated in Table 1, the observed peaks correspond to N–H stretch1°, 2^ amines, amides, C–H stretch alkanes, Nitrile C=N Stretch, C=C stretch (conjugated) alkenes, C-F stretch alkyl halides, C-N Amines, and C–Br stretch alkyl halides, respectively.

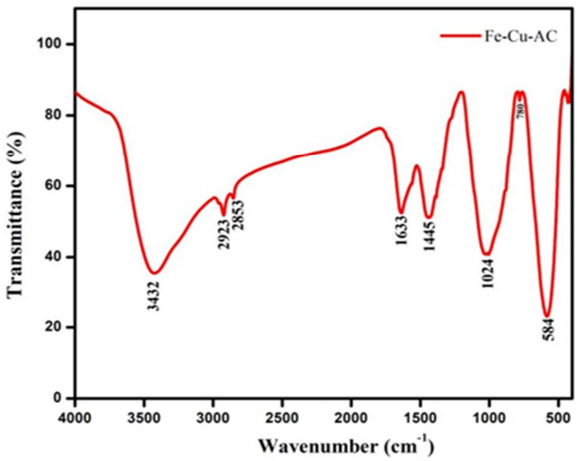

Fig. 6. FTIR spectrum of Cu Fe2O4/AC Nanocomposite

These bands represent stretching vibrational bands that are responsible for the formation of molecules

like as terpenoids and flavonoids, and hence they might be attributed to the effective stabilizing and capping of the resulting Cu Fe_2O_4/AC nanocomposite. The peaks showed that the Cu-Fe ions in the nanocomposites have several functional groups that were responsible for the stable Cu Fe_2O_4/AC nanocomposite production (Crini *et al.,* 2006).

Table 1. Peak table of Cu Fe2O4/AC NCs

SL	Peak (cm^{-1})	Functional group
1	3432	N–H stretch1°, 2° amines, amides
2	2923	C–H stretch alkanes
3	2853	Nitrile C≡N Stretch
4	1633	C=C stretch (conjugated) alkenes
5	1445	C-F stretch alkyl halides
6	1024	C-N Amines
7	584	C–Br stretch alkyl halides

Scanning electron microscopy (SEM) and EDAX

The SEM pictures of the Cu Fe_2O_4/AC nanocomposite are displayed in Fig. 7. SEM images provide evidence for the morphological behavior and structure of the bimetallic nanoparticles. Different types of Cu Fe_2O_4/AC nanocomposite were produced when NaOH was utilized as a capping and reducing agent. Cu-Fe NPs with approximately spherical agglomerated and indeterminate shapes were generated by the Cu Fe_2O_4/AC nanocomposite, respectively (Goldberg *et al.,* 2001). This may be because different capping agent types and quantities are present in different nanocomposites. This is further supported by the peaks' shifts and variations in regions discovered in the FTIR analysis.

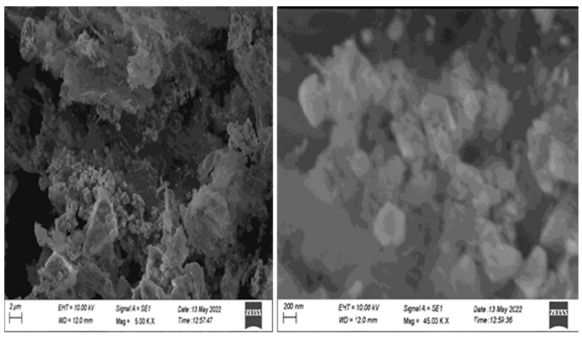

Fig.7. SEM image of Cu Fe_2O_4/AC nanocomposite

To comprehend the semi-quantitative elemental composition of the Cu Fe_2O_4/AC Nanocomposite, EDX analysis was performed (Fang *et al.,* 2010). The peaks indicated the presence of iron and copper particles (Fig. 8). In order to support the purity of metallic nanoparticles, the total metal content was rather high.

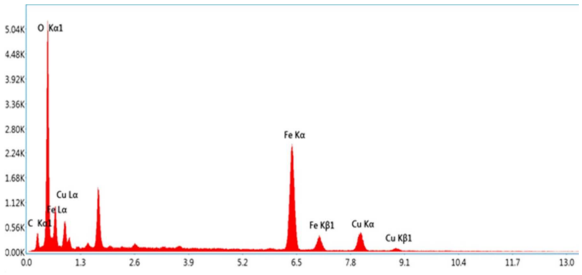

Fig. 8. EDAX spectrum of Cu Fe_2O_4/AC nanocomposite

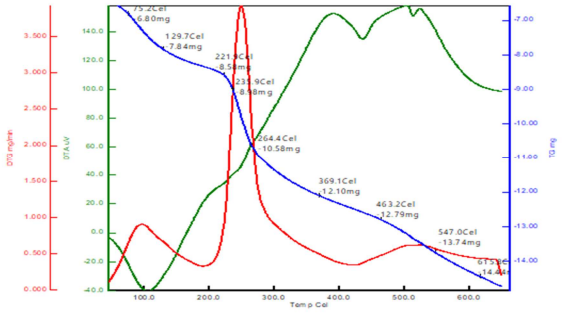

Fig.9. TGA analysis of Cu Fe_2O_4/AC nanocomposite

Thermogravimetric analysis (TGA)

Fig. 9 displays the TG analysis of the Cu Fe_2O_4/AC nanocomposite, which was created using Desmostachya bipinnata. The range of temperatures is 500–7000 degrees Celsius. The loss of nitrate compounds is correlated with the initial weight loss at 750°C. The breakdown of covalently bound organic material, namely nitrate, which was changed to oxide throughout the production process, is shown by the peak that was found after 2350°C. Cu Fe_2O_4/AC nanocomposite DTA curves exhibit an exothermic peak between 100°C and 300°C as a result of nitrate component desorption and breakdown (Arun *et al.,* 2017). When the initial weight loss in TG analysis is less than 75°C, it means that water evaporation occurred on the sample's surface. Peak rise over this temperature is caused by adsorption as a result of organic material that is covalently bound breaking down. The predicted weight loss of the resulting Cu Fe2O4/AC nanocomposite is 24.5%.

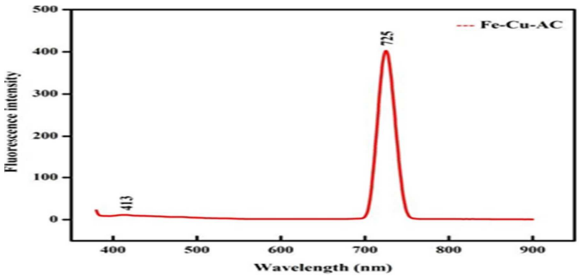

Fig. 10. Fluorescence spectrum of Cu Fe_2O_4/AC nanocomposite

Fluorescence spectroscopy (FL)

The fluorescence spectra of the Cu Fe_2O_4/AC Nanocomposite at room temperature were recorded using a fluorescence spectrophotometer, as illustrated in Fig. 10. The measurements were conducted between 400 and 900 nm in wavelength. As seen in Fig. 10, the experiments' maximum wavelength emission intensities were gathered, and emission values were displayed as wavelength (nm) versus intensity (A.U). Cu Fe_2O_4/AC Nanocomposite has two distinct peaks, as seen in Fig. 10 (Ahmed *et al.,* 2016). The formation of the Cu Fe_2O_4/AC Nanocomposite was ascribed to the lower emission peaks, measured at 413 nm, and the higher emission peak, detected at 725 nm. Surface imperfections were the cause of the higher emission peak, measured at 647 nm. In order to ascertain energy levels, fluorescence spectra were the preferred method. As the C Cu Fe_2O_4/AC Nanocomposite expanded in size, the fluorescence intensity rose.

Photocatalytic activities of Cu Fe_2O_4/AC nanocomposite for the degradation of methylene blue dye

As demonstrated in Fig. 11 a and b, the dye's degradation increased over time, peaking at 98 percent at 240 minutes. In the first five minutes, the degradation rose with an increase in UV light irradiation, reaching 5.6%. After examining the connection between deterioration and time, it's time to determine how it occurs. The mechanism was determined by examining the impact of time on the degrading process. Prior to being exposed to ultraviolet light, which excites valence electrons and permits them to move from the valence band to the conduction band, the dye is first adsorbed on the surface of the catalyst (in this case, Cu-Fe-AC NCs). During this process, a positive hole (h^+) is lifted inside the valence band (Prody *et al.,* 2019). Adsorbed water molecules on the surface of the photocatalyst will combine with the positive holes and free electrons to form ·OH radicals, while the free electrons will change the dissolved oxygen into superoxide anion O_2 • radicals. These light-generated radicals break down the dye molecules into simpler molecules like CO_2 and H_2O.

Cu Fe_2O_4/AC Nanocomposite + hν → e^- + h^+

$H2O + h^+ \rightarrow OH \cdot + H^+$

$O_2 + e^- \rightarrow O_2 \cdot -$

OH + dye → degradable product

O_2 – + dye → degradable product

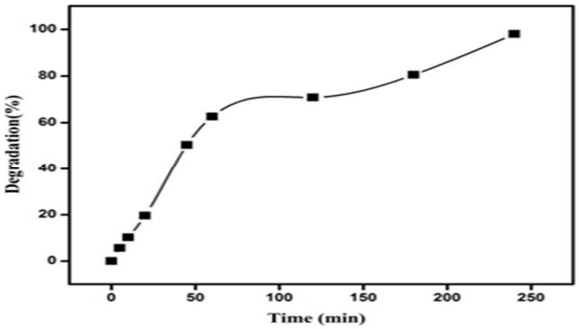

Fig. 11 a. Percent degradation of Methylene blue dye with Cu Fe2O4/AC nanocomposite

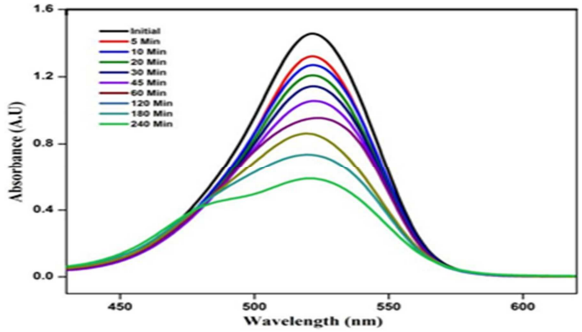

Fig. 11 b. UV–visible spectra of Cu Fe2O4/AC Nanocomposite

Antibacterial activity

Examining the antibacterial activity of the generated Cu Fe_2O_4/AC Nanocomposite and its dependence on the selected microbiological species—namely, *Staphylococcus aureus*, *Pseudomonas* sp., *Bacillus*

subtilis, *Enterobacter*, and *Escherichia coli* was the aim of this investigation. Numerous bacterial species displayed zones of inhibition in the well diffusion method of antibacterial activity. The different patterns of the zone of inhibitions are shown in Fig. 12, Table 2. The Cu Fe_2O_4/AC Nanocomposite exhibited antibacterial efficacy against both Gram-positive and Gram-negative pathogens (Rivera-Utrilla *et al.*, 2001). After a 24-hour culture, pathogenic bacteria were cultivated in nutrient broth and swabbed uniformly onto different plates with muller hinton agar using sterile cotton swabs. On all plates, the purified Cu Fe_2O_4/AC Nanocomposite was added to each well at different weights, including 25 ul, 50 ul, 75 ul, and 100 ul. The plates were incubated at 37°C for 24 hours in an incubator. After incubation, the different zones of formation surrounding the well were measured (Abdelwahab and Shukrg, 2014).

Adsorption kinetics

The kinetics of adsorption was studied for its possible importance in the treatment of dye-containing industrial effluents. Numerous kinetic models have been proposed to elucidate the mechanism by which pollutants are adsorbed. To investigate the mechanism of the dye adsorption kinetic models were considered as follows. The kinetics of adsorption is important from the point of view that it controls the process efficiency. Various kinetic models have been used by various workers and different systems conform to different models but the Langergrens rate equations (Ho and Mckay, 1998a; 1998b; 1999) for the sorption of a solute form liquid solution. In order to examine the controlling mechanism of adsorption processes such as mass transfer and chemical reaction, several kinetic models are used to test experimental data.

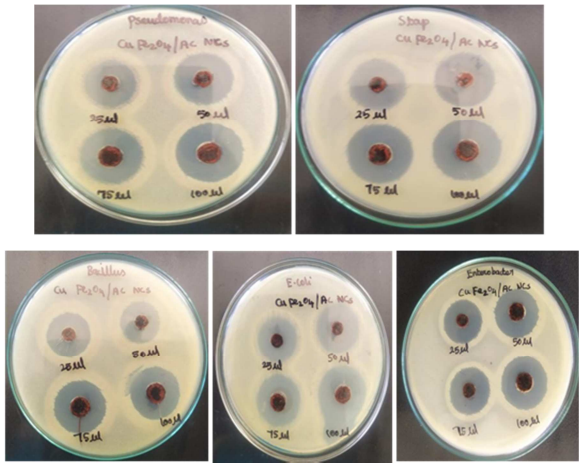

Fig. 12. Zone of inhibition of Cu Fe2O4/AC Nanocomposite various bacterial strains

Effect of dye concentration

Fig. 13 shows the effect of dye concentration on the Cu Fe_2O_4/AC Nanocomposite's ability to remove Methylene blue dye at starting concentrations of 20, 30, and 40 g/L when coupled with the nanocomposite. Since a particular mass of sorbent material may only adsorb a specific amount of dye, the initial dye concentration of an effluent is crucial (Benaāssa 2005; Bharathi and Ramesh, 2013).

Table 2. Zone of inhibition of Cu Fe_2O_4/AC nanocomposite against selected bacterial strains

	Zone of Inhibition (mm in diameter)				
Concentration	*Bacillus*sp.	*E. coli*	*Enterobacter* sp.	*Staphylococuus aureus*	*Pseudomonas* sp.
25 µl	1.7	1.8	1.8	1.8	1.7
50 µl	1.9	2	2.2	2.3	2.0
75 µl	2.5	2.5	2.7	2.5	2.6
100 µl	2.8	2.7	2.9	2.8	2.9

By creating an adsorbent–adsorbate solution with a fixed adsorbent dose and varying the initial dye concentration for various time intervals, then shaking the mixture until equilibrium, one can test the effect of initial dye concentration (Salleh *et al.*, 2011; Bharathi and Ramesh, 2013). According to Salleh *et al.* (2011) and Bharathi and Ramesh (2013), the instantaneous relationship between the dye concentration and the number of binding sites that are available on an adsorbent surface determines the effect of the initial dye concentration factor. As the initial dye concentration increases, the dye removal usually decreases. According to Low and Lee (1990), the

amount of dye that an adsorbent can absorb is fixed for a given mass of the adsorbent.

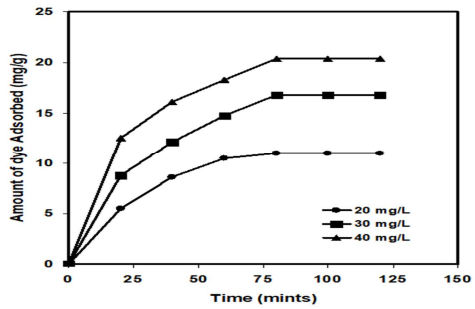

Fig. 13. Effect of specific dye uptake at different dye concentration with time (mints)

There will be vacant active sites on the adsorbent surface at low concentrations, and as the initial dye concentration rises, there won't be as many active sites available for the dye molecules to adsorb (Kannan and Sundaram 2001; Bharathi and Ramesh, 2013). According to Low and Lee (1990), as concentration grew, so did the amount of time needed to attain equilibrium. Yet, when dye concentration rose, so did the real amount of dye absorbed per unit mass of adsorbent. This might result from a high initial dye concentration and a strong driving force for mass transfer (Bulut and Aydin, 2006). However, Garg *et al.* (2004) found that at all dye concentrations under study, 100% of the dye was removed by granular activated carbon. Thus, the initial dye concentration has a significant impact on the adsorption. As the initial dye concentration rises, the adsorbent material's capacity is rapidly depleted. The fact that the total number of accessible adsorbent sites remains constant for all concentrations tested at a given adsorbent dose may be the cause of this. The amount of accessible adsorption sites decreases with concentration, hence the initial concentration determines the percentage of dye removed.

Effect of pH

Fig. 14 displays the proportion of dye adsorption at various pH values (5.5, 6.8, 7-8). By affecting the chemistry of the dye molecule and the adsorbents $CuFe_2O_4$/AC Nanocomposite in aqueous solutions, the initial pH of the Methylene blue dye solution has a significant impact, especially on the adsorption capacity. When Methylene Blue Dye is dissolved in water, its hue turns a solid red about pH 6.8. Methylene blue dye turns red at alkaline pH values (5.5, 6.8, 7-8) and dark blue at acidic pH values, but this red color is slightly different from original red at the neutral pH. At basic pH (sulfonate groups), methylene blue dye occurs as an anionic form; at acid pH, it exists as a cationic form. Cu Fe_2O_4/AC Nanocomposite was found to have a zero point charge of 6.8 (Rivera-Ultrilla *et al.*, 2001; Sumanjit *et al.*, 2013). According to Mall *et al.* (2006) and Sumanjit *et al.* (2013), adsorption of an anion is preferred at pH <, but adsorption of a cation is preferred when pH >. It was discovered that the values for the Cu Fe2O4/AC Nanocomposite were 5.5 and 6.8, respectively. As shown in Fig. 14, the percentage of dye adsorption in the case of the Cu Fe_2O_4/AC Nanocomposite decreased rapidly from 84 to 63% as the pH value of the dye solution increased from 2 to 12. The positively charged adsorbent surface and anionic dye exhibit a noticeably strong electrostatic attraction at pH 5.5. Both the quantity of negatively charged and positively charged sites rise and fall in proportion to the system's pH. Because of electrostatic repulsion, the adsorbent's negatively charged surface site is not favorable for the adsorption of dye anions. Additionally, excess ions competing with the dye anions for adsorption sites cause decreased Methylene blue dye adsorption at alkaline pH levels. However, because of a chemical interaction between the dye and the Cu Fe_2O_4/AC Nanocomposite, respectively, there was still a large amount of anionic dye adsorption on the adsorbent above. The adsorption of Congo red on waste orange peel and activated carbon has been reported to yield similar results (Namasivayam *et al.*, 1996; Sumanjit *et al.*, 2013). (Namasivayam and Kavitha, 2002; Sumanjit *et al.*, 2013). This could be because there are a lot of positive charges on the sorbent surface, which prevent the negatively charged dye molecule from being rejected and increase adsorption. Generally speaking, uptakes in acidic solutions are substantially higher than those in neutral and alkaline environments. This hypothesis is consistent with the

pH effect data we have. It is evident that the aqueous solution's pH has a significant impact on the methylene blue dye's ability to adhere to the Cu Fe_2O_4/AC Nanocomposite.

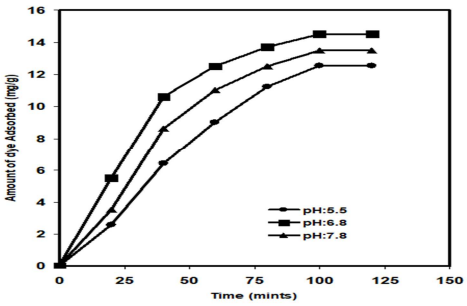

Fig. 14. Effect of specific dye uptake at different pH with time (mints)

In the adsorption process, pH is crucial, particularly for dye adsorption. The amount of electrostatic charges that the ionized dye molecules transfer depends on the pH of the medium. Therefore, the pH of an aqueous medium will affect the rate of adsorption (Onal *et al.* 2006; Bharathi and Ramesh, 2013). Dilute 0.1 N HCl or 0.1 N NaOH can be added to the initial dye solution to change its pH. In general, the proportion of dye removal for cationic dye adsorption will decrease in low pH solutions, but the percentage of dye removal for anionic dyes will increase. On the other hand, the proportion of dye removal for cationic dye adsorption would rise in a high pH solution, whereas the percentage for anionic dye adsorption will fall (Salleh *et al.* 2011; Bharathi and Ramesh, 2013). Elec trostatic repulsion between the positively charged dye and the adsorbent surface is lessened as surface charge density falls with increasing solution pH, potentially leading to an increase in the degree of adsorption (Wang *et al.*, 2006; Bharathi and Ramesh, 2013). The electrostatic repulsion between the positively charged cationic dyes and the adsorbent surface decreases as the pH of the solution rises, increasing the removal effectiveness (Ansari and Mosayebzadeh 2010; Bharathi and Ramesh, 2013). Changes in pH between 2 and 10 had no effect on the dye adsorption by coconut-based carbon, according to Garg *et al.* (2004). Maximum dye adsorption (96%) was seen in sawdust treated with sulfuric acid at pH values between 6 and 10, with a reduction to 70% at pH 2.0. At a pH of 2.0, formal dehyde-treated sawdust removed the least amount of color (26.8%), and at a pH of 10, it climbed to 100%. To learn more about the adsorption mechanism, numerous researchers examined the isoelectric point (pHIEP) of adsorbents made from agricultural solid wastes. Because of the existence of functional groups like OH- and COO groups, cationic dye adsorption is preferred at pH<[pHpzc. At pH<pHpzc, where the surface becomes positively charged, anionic dye adsorption is favored (Radovic *et al.*, 1997; Bharathi and Ramesh, 2013). The adsorbent surface appears negatively charged in high pH solutions, as the positive charge at the solution interface diminishes (Ozcan *et al.*, 2007; Bharathi and Ramesh, 2013). Consequently, there is an increase in cationic dye adsorption and a decrease in anionic dye adsorption (Salleh *et al.*, 011; Bharathi and Ramesh, 2013). According to Zawani *et al.* (2009), the optimal pH for Remazol black 5 adsorption on palm kernel shell activated carbon is 2, and the highest absorption occurs at 27.44 mg g-1. After that, there is a significant drop in uptake. The carbon surface dye binding sites and the dye chemistry in water are both influenced by the pH of the solution. The carbon will have a net positive charge at lower pH levels. The electrostatic interactions between the positively charged adsorbent surface and the negatively charged functional groups on the reactive dye may be the cause of the higher uptakes observed at lower pH values. Additionally, the hydrogen ion serves as a bridging ligand to connect the dye molecule to the adsorbent wall.

Effect of temperatures

Cu Fe_2O_4/AC Nanocomposite sorption tests were reported at three different temperatures: 300C, 450C, and 600C. Fig.15 indicates that the amount of color removed increases as temperature rises, suggesting that methylene blue dye is best removed from aqueous solutions at high temperatures. Raising the temperature causes the dye to become less soluble, which leads to an increase in adsorption. The big dye ion's increased mobility with temperature could

possibly be the cause of increased adsorption. More and more molecules might have enough energy to engage with the surface's active site (Dogan and Alkan, 2003; Sumanjit *et al.*, 2013). Consequently, chemisorptions may be partially responsible for the rise in the sorptive absorption of methylene blue dye with temperature. An essential element of the adsorption process is temperature. Important information regarding the enthalpy and entropy changes during adsorption can be learned from a study of the temperature dependence of adsorption reactions (Dogan and Alkan, 2003; Bharathi and Ramesh, 2013). Temperature is an indicator for the adsorption nature whether it is an exothermic or endothermic process (Salleh *et al.* 2011; Bharathi and Ramesh, 2013). Adsorption is considered to be an endothermic process if its capacity rises with temperature. This could be because as the temperature rises, the mobility of the dye molecules increases and there are more active sites available for adsorption (Senthilkumaar *et al.*, 2006; Bharathi and Ramesh, 2013). According to Senthilkumaar *et al.* (2006), activation of the adsorbent surface and pore size enlargement are responsible for the increased adsorption capacity of activated carbon at higher temperatures. Certain structural alterations in the dyes and the adsorbent take place there during the adsorption process (Hema and Arivoli 2007; Bharathi and Ramesh, 2013). The system is made more random by the adsorbed water molecules, which are displaced by the adsorbate species, gaining more translational entropy than the adsorbate mole cules lose. Due to a loss in adsorption capacity, rising temperatures may result in a decrease in the adsorptive forces between the dye species and the active sites on the adsorbent surface (Oladoja *et al.*, 2008; Bharathi and Ramesh, 2013).

Fig. 15 displays a plot showing the uptake of Methylene blue dye as a function of temperature (30, 45, and 600C). It was discovered that dye adsorption was higher at higher temperatures than it was at lower ones. The curves show a clear tendency for the process to create monolayers (Namasivayam and Kavitha, 2002; Namasivayam *et al.*, 1998; 2001).

As a result, the chemical interaction between the functional groups on the adsorbent surface and the adsorbate should be the primary determinant of the adsorption capacity, which should rise as temperature does.

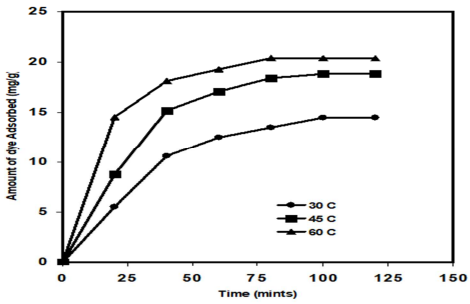

Fig. 15. Effect of specific dye uptake at different temperature with time (mints)

From a system design viewpoint, a lumped analysis of adsorption rates is thus sufficient to practical operation. A simple kinetic analysis of adsorption is the pseudo-first-order equation;

$$\frac{dq_t}{q_t} = K_1\left(q_{eq} - q_t\right) \quad (3)$$

After definite integration by applying the initial conditions qt=0 at t=0 and qt=qt at t=t, equation (3) becomes;

$$\log\left(q_{eq} - q_t\right) = \log q_{eq} - \frac{K_1}{2.303}t \quad (4)$$

Where qeq and qt are amount of dye adsorbed at equilibrium and at time, in mg g-1 respectively, and K1 is the first order rate constant, was applied to the present studies of dye adsorption. As such the values of log (qe-qt) vs t were calculated form the kinetic data of (Fig. 16-18) and plotted against time. The first-order rate constant calculated form the plots k1 (mg g-1 min-1) and qeq (mg g-1 min-1) values are shown in (Table 3). Adsorption kinetics for some system can also be described by a pseudo-second order reaction.

The pseudo-second-order equation based on adsorption equilibrium capacity may be expressed in the form;

$$\frac{dq_t}{q_t} = K_2 (q_{eq} - q_t)^2 \quad (5)$$

Where k_2 is the rate constant of pseudo-second-order adsorption. Integrating equation (4) and applying the initial conditions, we have

$$\frac{1}{(q_{eq} - q_t)} = \frac{1}{q_e} + K_2 t \quad (6)$$

or equivalently,

$$\frac{t}{q_t} = \frac{1}{K_2 q_{eq}^2} + \frac{1}{q_e} t \quad (7)$$

The equilibrium adsorption capacity (q_{eq}), and the second-order constants k_2 (g/mg min) can be determined experimentally from the slope and intercept of plot t/q_t versus t.

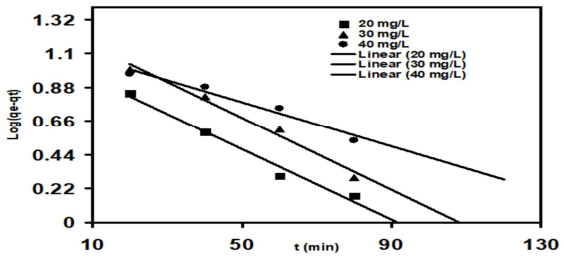

Fig. 16. Pseudo-first order plot for the adsorption of dye using Cu Fe2O4/AC Nanocomposite at various plot at Dye concentration

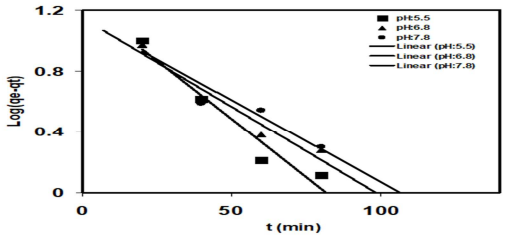

Fig. 17. Pseudo-first order plot for the adsorption of dye using Cu Fe2O4/AC Nanocomposite at various plot at pH

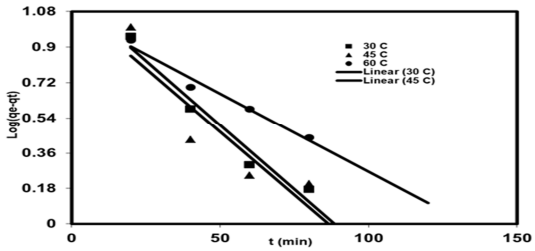

Fig. 18. Pseudo-first order plot for the adsorption of dye using Cu Fe2O4/AC Nanocomposite at various plot at pH

Table 3. Pseudo-first and Pseudo-Second order rate constant at different dye concentration, pH and temperature

Dye conc. (mg/L	Pseudo-first order rate constant	Pseudo-Second order rate constant
20	K_1= 0.0264;	K_2=0.002;
	q_{eq}= 1.049	q_{eq}= 16.86;
	R^2= 0.9771	R^2= 0.9929
30	K_1= 0.026;	K_2= 0.0009;
	q_{eq}= 1.264;	q_{eq}= 25.12;
	R^2= 0.9832	R^2= 0.9918
60	K_1= 0.016582;	K_2= 0.0014;
	q_{eq}= 1.1423;	q_{eq}= 27.93;
	R^2= 0.9625	R^2= 0.9781
pH	Pseudo-first order rate constant	Pseudo-Second order rate constant
5.5	K_1= 0.0352;	K_2=0.001;
	q_{eq}= 1.249;	q_{eq}= 16.50;
	R^2= 0.9473	R^2= 0.9863
6.8	K_1= 0.0246;	K_2=0.002;
	q_{eq}= 1.148;	q_{eq}=17.98;
	R^2= 0.9490	R^2= 0.9937
7.8	K_1= 0.0246;	K_2=0.001;
	q_{eq}= 1.427	q_{eq}=18.38 ;
	R^2= 0.9082	R^2= 0.9598
Temp. (°C)	Pseudo-first order rate constant	Pseudo-Second order rate constant
30	K_1= 0.0301	K_2=0.001;
	q_{eq}= 1.159;	q_{eq}=20.74;
	R^2= 0.9586	R^2= 0.9687
45	K_1=0.029;	K_2=0.002;
	q_{eq}= 1.1137;	q_{eq}=26.88;
	R^2= 0.8180	R^2= 0.9888
60	K_1= 0.0184;	K_2=0.002;
	q_{eq}= 1.064;	q_{eq}=23.25;
	R^2= 0.9750	R^2= 0.9793

The applicability of the pseudo-second order models can be examined by linear plot t/q vs t respectively as shown in (Fig.19-21). The correlation coefficient R^2 shows that the pseudo-second order model an indications of a chemisorptions mechanism, fits the experimental data slightly better than the pseudo-first order model. Therefore the adsorption of methylene blue dye can be approximated more favorably by the pseudo-second order model. This model has been successfully applied to describe the kinetics of many adsorption systems. Calculated correlations are closer to unity for second-order kinetics model; therefore the adsorption kinetics could well be approximated more favourably by second-order kinetic model for dye adsorption. The k_2 (mg g^{-1} min^{-1}) and q_{eq} (mg g^{-1} min^{-1}) values as calculated are listed in (Table 3).

Conclusion

The goal of this study is to develop a one-pot eco-friendly chemical-based synthesis of Cu Fe_2O_4/AC

Nanocomposite. $CuFe_2O_4$/AC Nanocomposite has been synthesized by hydrothermal method. The crystalline structure of the produced NPs was confirmed by XRD examination. The presence of activated carbon involved in the transfer of metallic ions to NPs was confirmed using Fourier transform infrared (FTIR) spectroscopy. SEM was used to assess morphologies and vibrational modes, DLS was used to determine surface charge and stability, and TGA was used to determine stability. Synthesized Cu Fe_2O_4/AC Nanocomposite has shown successful capacity for against bacterial strains. The synthesized Cu Fe_2O_4/AC Nanocomposite was also effective in the degradation of Methylene blue dye. Controlling the ratio of Cu Fe_2O_4/AC Nanocomposite is very important to obtain good electrochemical performance. Kinetic studies were made for the adsorption of Methylene blue from aqueous solutions onto a Cu Fe_2O_4/AC Nanocomposite. This adsorbent exhibited high sorption capacities: the monolayer adsorption capacities were 20 mg/L (342.4mg/g); pH : 6.8 (28.4mg/g), 60°C (34.6 mg/g) of dye per gram of Cu Fe_2O_4/AC Nanocomposite respectively. The straight lines in plots of t/qt versus t showed good agreement of experimental data with the second-order kinetic model for different initial sorbent concentration, suggesting that the adsorption process might be chemisorption and physicalsorption. The present research work established that Cu Fe_2O_4/AC Nanocomposite were excellent low-cost bioadsorbents for the removal of dye methylene blue. The kinetics data can be further explored for the design of an adsorber for industrial effluents treatment.

References

Abdelwahab NA, Shukry N. 2014. Synthesis, characterization and antimicrobial properties of grafted sugarcane bagasse/silver nanocomposites. Carbohydrate Polymers **115**, 276-284.

Ahmed S, Ahmad M, Swami BL, Ikram S. 2016. A review on plants extract mediated synthesis of silver nanoparticles for antimicrobial applications: a green expertise. Journal of Advanced Research **7(1)**, 17-28.

Ahn CH, Choi JW, Cho HJ. 2004. Encyclopedia of Nanoscience and Nanotechnology; Nalwa, H.S., Ed.; American Scientific Publishers: Stevenson Ranch, CA, USA. **6**, 815.

Amit K, Changsheng G, Gaurav S, Deepak P, Mu N, Susheel KPD. 2016. Magnetically recoverable ZrO2/Fe3O4/chitosan nanomaterials for enhanced sunlight driven photoreduction of carcinogenic Cr(VI) and dechlorination & mineralization of 4-chlorophenol from simulated wastewater. RSC Advances **6**, 13251-13263.

Ansari R, Mosayebzadeh Z. 2010. Removal of basic dye methylene blue from aqueous solutions using sawdust and sawdust coated with polypyrrole. Journal of the Iranian Chemical Society **7**, 339-350.

Arun M, Panicker K, Rajesh T, Varghese O. 2017. Mixed morphology nanocrystalline cellulose from sugarcane bagasse fibers/poly(lactic acid) nanocomposite films: synthesis, fabrication and characterization. Iranian Polymer Journal **25**, 125-136.

Bello OS, Adelaide OM, Hammed MA, Popoola OAM. 2010. Kinetic and equilibrium studies of methylene blue removal from aqueous solution by adsorption on treated sawdust. Macedonian Journal of Chemistry and Engineering **29**, 77-85.

Benaissa H. 2005. Removal of acid dyes from aqueous solutions using orange peel as a sorbent material. Ninth International Water Technology Conference, IWTC9, Sharm El-Sheikh, Egypt. 1175-1185.

Bharathi KS, Ramesh ST. 2013. Removal of dyes using agricultural waste as low-cost adsorbents: a review. Applied Water Science **3**, 773-790.

Boudrahem F, Soualah A, Aissani-Benissad F. 2011. Pb(II) and Cd(II) removal from aqueous solutions using activated carbon developed from coffee residue activated with phosphoric acid and zinc chloride. Journal of Chemical Engineering Data **56**, 1946-1955.

Choi JH. 2010. Fabrication of a carbon electrode using activated carbon powder and application to the capacitive deionization process. Separation and Purification Technology **70**, 362-366.

Crini G, Peindy HN. 2006. Adsorption of CI. Basic Blue 9 on cyclodextrin-based material containing carboxylic groups. Dyes and Pigments **70**, 204-211.

Dogan M, Alkan M. 2003. Adsorption kinetics of methyl violet onto perlite. Chemosphere **50(4)**, 517-528.

Fang L, Zu X, Liu C, Li Z, Peleckis G, Zhu S, Liu H, Wang L. 2010. Microstructure and magnetic properties in Sn1–xFexO2 (x = 0.01, 0.05, 0.10) nanoparticles synthesized by hydrothermal method. Journal of Alloys and Compounds **491(1-2)**, 679-683.

Garg VK, Rakesh K, Renuka G. 2004. Removal of Malachite green dye from aqueous solution by adsorption using agro-industry waste: a case study of Prosopis cineraria. Dyes and Pigments **62**, 1-10.

Gokce Y, Aktas Z. 2014. Nitric acid modification of activated carbon produced from waste tea and adsorption of methylene blue and phenol. Applied Surface Science **313**, 352-359.

Goldberg M, Langer R, Jia X. 2007. Nanostructured materials for applications in drug delivery and tissue engineering. Journal of Biomaterials Science, Polymer Edition **18**, 241-268.

Gregorio C. 2008. Kinetic and equilibrium studies on the removal of cationic dyes from aqueous solution by adsorption onto a cyclodextrin polymer. Dyes and Pigments **77**, 415-426.

Han Z, Dong Y, Dong S. 2011. Copper-iron bimetal modifies PAN fiber complexes as novel heterogeneous Fenton catalyst for the degradation of organic dye under visible light irradiation. Journal of Hazardous Materials **189**, 241-248.

Hema M, Arivoli S. 2007. Comparative study on the adsorption kinetics and thermodynamics of dyes onto acid activated low cost carbon. International Journal of Physical Sciences **2**, 10-17.

Ho YS, McKay G. 1998a. Kinetic models for the sorption of dye from aqueous solution by wood. Process Safety and Environmental Protection **76**, 183-191.

Ho YS, McKay G. 1998b. Sorption of dye from aqueous solution by peat. Chemical Engineering Journal **70**, 115-124.

Ho YS, McKay G. 1999. A kinetic study of dye sorption by biosorbent waste product pith. Resources Conservation Recycling **25**, 171-193.

Huang W, Zhang Y, Bao S, Cruz R, Song S. 2014. Desalination by capacitive deionization process using nitric acid-modified activated carbon as the electrodes. Desalination **340**, 67-72.

Jin X, Liang Y, Wang J, Wang Q, Wu Y, Chong WWF, Sonne C, Lam SS, Xia C. 2023. Hierarchical self-assembly of polyphenolic functionalized magnetic superstructure for enhanced removal of organic dyes. Journal of Chemical Engineering **457**, 141142.

Khenniche L, Benissad-Aissani F. 2010. Adsorptive removal of phenol by coffee residue activated carbon and commercial activated carbon: equilibrium, kinetics, and thermodynamics. Journal of Chemical Engineering Data **55**, 4677-4686.

Liu QS, Zheng T, Li N, Wang P, Abulikemu G. 2010. Modification of bamboo-based activated carbon using microwave radiation and its effects on the adsorption of methylene blue. Applied Surface Science **256**, 3309-3315.

Low KS, Lee CK. 1990. The removal of cationic dyes using coconut husk as an adsorbent. Pertanika **132**, 221-228.

Lozano-Castello D, Lillo-R.Odenas M, Cazorla-Amorós D, Linares-Solano A. 2001. Preparation of activated carbons from Spanish anthracite: I. Activation by KOH. Carbon **39**, 741-749.

Mall ID, Srivastava VC, Kumar GV, Mishra IM. 2006. Characterization and utilization of mesoporous fertilizer plant waste carbon for adsorptive removal of dyes from aqueous solution. Colloids and Surfaces A **278(1-3)**, 175-187.

Mi J, Wang XR, Fan RJ, Qu WH, Li WC. 2012. Coconut-shell-based porous carbons with a tunable micro/mesopore ratio for high-performance supercapacitors. Energy and Fuels **26**, 5321-5329.

Mohanty K, Naidu JT, Meikap BC, Biswas MN. 2006. Removal of crystal violet from wastewater by activated carbons prepared from rice husk. Industrial & Engineering Chemistry Research **45**, 5165-5171.

Namasivayam C, Kavitha D. 2002. Removal of Congo Red from water by adsorption onto activated carbon prepared from coir pith, an agricultural solid waste. Dyes and Pigments **54(1)**, 47-58.

Namasivayam C, Muniasamy N, Gayatri K, Rani M, Ranganathan K. 1996. Removal of dyes from aqueous solutions by cellulosic waste orange peel. Bioresource Technology **57(1)**, 37-43.

Namasivayam C, Prabha D, Kumutha M. 1998. Removal of direct red and acid brilliant blue by adsorption on to banana pith. Bioresource Technology **64(1)**, 77-79.

Namasivayam C, Radhika R, Subha S. 2001. Uptake of dyes by a promising locally available agricultural solid waste: Coir pith. Waste Management **38**, 381-387.

Oladoja NA, Aboluwoye CO, Oladimeji YB. 2008. Kinetics and isotherm studies on methylene blue adsorption onto ground palm kernel coat. Turkish Journal of Engineering and Environmental Science **32**, 303-312.

Onal Y, Akmil-Basar C, Eren D, SarIcI-Ozdemir C, Depci T. 2006. Adsorption kinetics of Malachite green onto activated carbon prepared from Tunc¸bilek lignite. Journal of Hazardous Materials **128**, 150-155.

Onundi YB, Mamun AA, Khatib MFA, Ahmed YM. 2010. Adsorption of copper, nickel and lead ions from synthetic semiconductor industrial wastewater by palm shell activated carbon. International Journal of Environmental Science and Technology **7**, 751-758.

Ozcan A, O¨meroglu C, Erdogan Y, Ozcan AS. 2007. Modification of bentonite with a cationic surfactant: an adsorption study of textile dye Reactive Blue 19. Journal of Hazardous Materials **140**, 173-179.

Piyush K, Yun Z, Najia M, Ujwal KT, Benjamin DW, Ryan K, Karthik S. 2018. Heterojunctions of mixed phase TiO2 nanotubes with Cu, CuPt, and Pt nanoparticles: interfacial band alignment and visible light photoelectrochemical activity. Nanotechnology **29**, 014002.

Prodyut D, Bruna P, Antonio J, Gonçalves C, Sandip B, Sakamoto S, Imai HJ, Shiraishi Y, Tanaka S, Ichikawa S, Hirai T. 2019. Photocatalytic dehalogenation of aromatic halides on Ta2O5-supported Pt–Pd bimetallic alloy nanoparticles activated by visible light. ACS Catalysis **7**, 5194-5201.

Radovic LR, Silva IF, Ume JI, Menendez JA, Leon CA, Leon Y, Scaroni AW. 1997. An experimental and theoretical study of the adsorption of aromatics possessing electron withdrawing and electron-donating functional groups by chemically modified activated carbons. Carbon **35**, 1339-1348.

Rivera-Utrilla J, Bautista-Toledo I, Ferro-Garcia MA, Moreno-Castilla C. 2001. Activated carbon surface modifications by adsorption of bacteria and their effect on aqueous lead adsorption. Journal of Chemical Technology and Biotechnology **76(12)**, 1209-1215.

Salleh MAM, Mahmoud DK, Karim WAWA, Idris A. 2011. Cationic and anionic dye adsorption by agricultural solid wastes: a comprehensive review. Desalination **280**, 1-13.

Sarasidis VC, Plakas KV, Karabelas AJ. 2017. Novel water-purification hybrid processes involving in-situ regenerated activated carbon, membrane separation and advanced oxidation. Journal of Chemical Engineering **328**, 1153-1163.

Sawant SY, Munusamy K, Somani RS, John M, Newalkar BL, Bajaj HC. 2017. Precursor suitability and pilot scale production of super activated carbon for greenhouse gas adsorption and fuel gas storage. Journal of Chemical Engineering **315**, 415-425.

Sekirifa ML, Hadj-Mahammed M, Pallier S, Baameur L, Richard D, Al-Dujaili AH. 2013. Preparation and characterization of an activated carbon from a date stones variety by physical activation with carbon dioxide. Journal of Analytical and Applied Pyrolysis **99**, 155-160.

Senthilkumaar S, Kalaamani P, Subburaam CV. 2006. Liquid phase adsorption of crystal violet onto activated carbons derived from male flowers of coconut tree. Journal of Hazardous Materials **136**, 800-808.

Sumanjit K, Seema R, Rakesh KM. 2013. Adsorption kinetics for the removal of hazardous dye Congo red by biowaste materials as adsorbents. Journal of Chemistry **628582**, 1-12.

Taer E. 2019. Preparation of activated carbon electrode from pineapple crown waste for supercapacitor application. International Journal of Electrochemical Science **14**, 2462-2475.

Zawani Z, Luqman Chuah A, Choong TSY. 2009. Equilibrium, kinetics and thermodynamic studies: adsorption of Remazol black 5 on the palm kernel shell activated carbon PKS-AC. European Journal of Science Research **37**, 67-76.

Zhou J, Luo A, Zhao Y. 2018. Preparation and characterisation of activated carbon from waste tea by physical activation using steam. Journal of the Air and Waste Management Association **68**, 1269-1277.